Integration of Magnetic Nanoparticles into 2D- and 3D-printed Nano-/Microstructures

G. MATHEW[a], E. LEMMA[b], M. HIRTZ[a] AND E. BERGANZA*[a,c]

[a]Institute of Nanotechnology (INT), Karlsruhe Institute of Technology (KIT), Hermann-von-Helmholtz-Platz 1, 76344 Eggenstein-Leopoldshafen, Germany; [b]Università Campus Bio-Medico di Roma, Via Álvaro del Portillo, 21, 00128 Rome, Italy; [c]Instituto de Ciencia de Materiales de Madrid, Sor Juana Ines de la Cruz 3, 29048 Madrid, Spain
*E-mail: eider.berganza@csic.es

14.1 Introduction

Due to their unique properties, the applications of magnetic nanoparticles (MNPs) cover a broad spectrum, which has been evolving in the last two decades to meet the changing societal demands. The enormous flexibility in the obtention of different sizes, shapes and compositions, together with their superparamagnetic behaviour, catalytic properties, *etc*., makes them good candidates for their integration into devices of different natures. In particular, the interest to position MNPs in ordered templates sparked two decades ago as a response to building high-density data storage devices, and many studies addressed their self-assembly (SA) on surfaces. Later, their integration into devices such as sensors or their use in catalysis leads to the need to print them into 2D architectures and the development of lithographic techniques towards this aim. Currently, further development

of printing technologies has pushed the creation of smart microrobots, often taking inspiration from multifunctional micromachines in nature, which drive the trend to exploit MNPs as functional elements integrated into 3D-printed architectures. In this chapter, we review advances in the controlled, digital generation of patterns and structures from MNPs. Nevertheless, as many of the later described approaches heavily rely on SA, we will first briefly discuss some key concepts relevant to the described techniques.

14.2 Concepts in MNP Self-assembly

During the past years, much effort has been devoted to the fundamental study and synthesis methods of MNPs.[1,2] Less attention has been paid to their SA onto surfaces, a process driven by an energy minimization trend from a disordered state to an ordered state, despite the relevance of the implications that this might have on the design of theranostic[1] or data storage devices.[3,4] For the present chapter, we limit our discussion specifically to the concepts used in MNP self-assembly to form surface-bound structures (in particular, excluding self-assembly synthesis of dispersed MNPs itself or the build-up of superstructures of MNPs by self-assembly in a solution without controlled transfer to a surface, thus not forming regular long-range surface patterns). In general, two main classes of MNP SA can be defined: (1) *template-free SA,* which nevertheless leads to long-range ordered regular surface patterns, and (2) *SA on pre-patterns*, which can be of chemical, topographical or magnetic nature. Both categories are often assisted by an external magnetic field.[5] A schematic overview of these categories is depicted in Figure 14.1.

Template-free SA relies on inter-particle interactions, *e.g.* by magnetic forces, or chemical interactions between MNP ligands and/or external driving in the form of magnetic or electrical fields. *SA on templates* generally involves specific interactions between the MNPs and certain areas of a surface that were rendered either attractive or repulsive towards the MNPs, by *e.g.* chemical modification or magnetic orientation. In the case of topographical templates, either pinning effects caused by surface geometry or subsequent mechanical removal of exposed areas of the template is utilized to obtain MNP surface patterns.

Later in the chapter, we will discuss the generation of MNP surface structures by digital printing techniques (being the focus of our review); however, we will briefly highlight a few examples of template-free SA and SA on non-printed pre-patterns in the following sections.

14.2.1 Template-free Self-assembly

Template-free SA can generate highly ordered surface patterns over large areas. Here, Wen and Majetich[8] demonstrated the coating of square

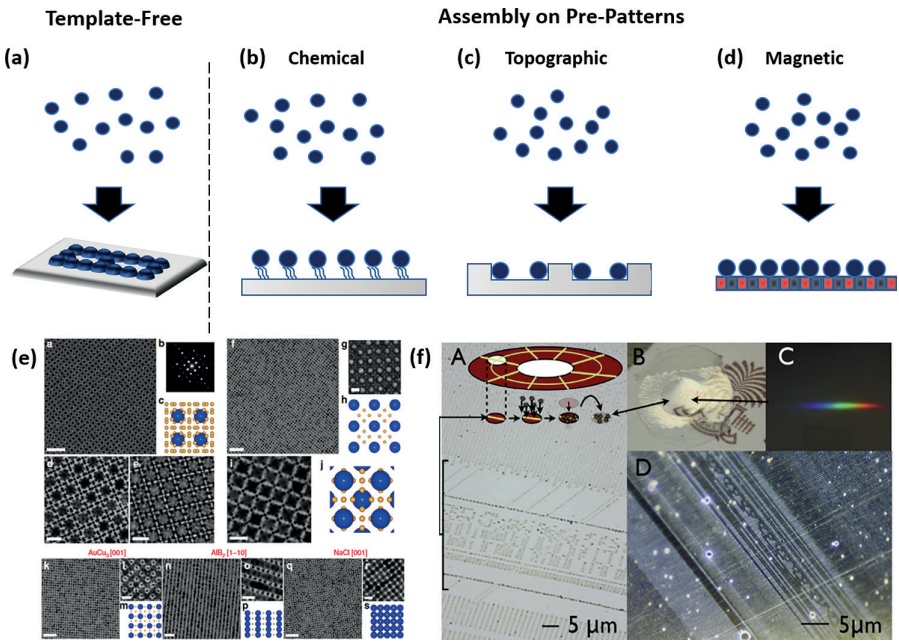

Figure 14.1 (a–d) Categories of MNP self-assembly. Examples of structures obtained *via* (e) template-free self-assembly. Reproduced from ref. 6, https://doi.org/10.1038/ncomms10052, under the terms of the CC BY 4.0 license, https://creativecommons.org/licenses/by/4.0/; and (f) assembly on a magnetic pre-pattern. Reproduced from ref. 7 with permission from IOP Publishing, Copyright 2012.

centimetre range surface areas with densely packed Fe_3O_4 MNPs (~12 nm). This was achieved by the controlled evaporation of an MNP solution in a binary solvent system (hexane/toluene) on a water subphase with subsequent Langmuir–Schaefer transfer of the formed film to a solid substrate. The approach allows for the creation of double layers with varying rotation angles, giving rise to Moiré patterns.[8]

In a different approach, Ye *et al.*[6] showed the formation of long-ranged-ordered binary nanocrystal superlattices of different monodisperse Au (3.8–7.6 nm) and 13.4 nm Fe_3O_4 NPs with polystyrene brush coating (Figure 14.1e). These lattices formed at the interface of a toluene solution containing the NPs and an immiscible diethylene glycol (DEG) subphase but could be transferred onto solid supports. Careful tuning of the NP interaction potential can be achieved by varying the molecular weight of the grafted polymer brushes on the NP surface, which yields the formation of 10 different 2D and 3D superlattices.[6]

Template-free methods can also result in even more complex structures by additional forcing. Singh *et al.* reported the formation of belt-like and helical superstructures crystalizing from Fe_3O_4 MNPs, driven by the

interplay between magnetic interactions (shape and magnetocrystalline anisotropy plus Zeeman coupling) and short-range interactions (van der Waals and entropic forces). The importance of magnetocrystalline anisotropy is proved by the use of NPs with different geometries (truncated octahedra, rounded cubes or cubic heterodimers with round Ag NPs), which form superstructures with varying shapes that have been transferred to solids, forming regular arrays of superstructures.[9] In addition, combinations of electric and magnetic fields were used to assist SA. For instance, Preger *et al*. used this approach to guide the SA of aerosolized charged MNPs. Here, they could produce different structures, ranging from one-dimensional nanochains to macroscopic three-dimensional networks, and can tune the alignment by changing the orientation of the external fields.[10]

Interesting information on the self-assembled layer formation of MNPs on surfaces was studied *via* neutron reflectometry (NR) on several occasions.[11] Theis-Bröhl *et al*. explored the SA of oleic acid (OA)-coated Fe_3O_4 MNPs (11 nm) on silicon surfaces with a native oxide layer. The authors compared the influence of a magnetic field as well as shear forces applied by a flow cell to free SA of the MNPs. For the free assembly under static conditions, they found a densely packed wetting layer on the sample surface consisting of an OA double layer with embedded ligand shell of the MNPs in a hexagonal order. Additionally, less dense layers formed on top of this wetting layer. For both, a magnetic field parallel to the surface, or under shear force, of the wetting layer was observed, indicating its high stability, although it was slightly compressed under the magnetic field (attributed to the alignment of the long axis of slightly elliptical NPs with the direction of the torque) and slightly thickened under shear force. The additional layers were not stable under shear force, with a depletion zone forming over the wetting layer.[12] Later, Theis-Bröhl *et al*.[13] studied the SA of 25 nm COOH-terminated Fe3O4 MNPs on (3-aminopropyl)triethoxysilane (APTES)-functionalized silicon surfaces from a water-based ferrofluid in a high and low (100 mT *vs.* 6 mT) magnetic field. They observed the emergence of a closely packed wetting layer of MNPs, with additional layers initially forming with close packing as well, but subsequently become less dense. Interestingly, these less dense layers (with the concentration comparable to the free ferrofluid) eventually dominate the overall magnetization, as the MNPs are free to rotate and, thus, decide the magnetization orientation. The additional freedom for rotation also results – though both wetting and free layer magnetizations align with the external in-plane field direction – in an anti-parallel alignment of the intermediate bound layers. In the high-field case, the intermediate region breaks into two layers with magnetization now pointing into different directions, attributed to possible in-plane quasi-domain formation by dipolar coupling, to minimize the free energy reducing the overall magnetization.[13] Saini *et al*. showed different surface-dependent outcomes for the assembly of *N*-hydroxysuccinimide ester (NHS)-coated MNPs of different sizes (5–25 nm) from water-based

ferrofluids onto functionalized silicon wafers. They found no layer built up on octadecyltrichlorosilane (OTS)-functionalized surfaces, as hydrophobic repulsion hinders the attachment of the MNPs. On piranha-treated and thus strongly hydrophilic surfaces, a wetting layer of MNPs can attach by physisorption, but chemisorption of the MNPs on an APTES-functionalized surface results in a denser layer. Overall, layers obtained from larger MNPs resulted in denser assemblies, which is observed for larger NPs with a ferrimagnetic behaviour, which can align their magnetization with the applied field *via* Brownian relaxation. Introducing an external magnetic field then allows for the build-up of additional layers and additional densification.[14]

14.2.2 Self-assembly on Pre-patterns

In most MNP SA approaches involving chemical pre-patterns, they are created with different types of printing techniques and will be discussed later in the chapter, together with the specific techniques. Here, we briefly exemplify the non-chemical, non-printed pre-pattern-based SA of MNPs (Figure 14.1c and d). Mechanical templates were used *e.g.* by Chen *et al.* in the form of regular nanopit arrays generated by electron- and ion-beam lithography. Regular arrays of different MNPs (Fe_3O_4, ~50 nm; FeO/$CoFe_2O_4$ with ~18 nm) could be achieved by drop-casting and drying a colloid solution of the MNPs (allowing SA into a densely packed monolayer) with subsequent removal of the MNPs in between the nanopits by polishing (similar to the Damascene process in semiconductor manufacturing). The approach can work independently of MNP size or ligand chemistry, allowing for even single MNP arrays by tuning the cavity size.[15] The use of magnetic pre-patterns as templates evolved out of the longstanding method to explore inhomogeneities in the magnetic field of materials by MNP SA, as the resulting assemblies could be observed even by optical microscopy.[16] With the advances in surface patterning techniques, this approach was then used for building up arbitrary MNP patterns. In 1993, Porthun *et al.* used this to visualize bit tracks written on Co–Cr data-recording media. Although their focus lay on imaging magnetic properties, this could also seen as an early MNP pattern generation with sub-100 nm features.[17] Saini *et al.* observed the SA of superparamagnetic (5 nm) and single-domain, ferromagnetic spherical Fe_3O_4 MNPs (15 nm and 25 nm) on a ferromagnetic $Tb_{15}Co_{85}$ substrate with an out-of-plane anisotropy. The combined NR and scanning electron microscopy (SEM) measurements reveal patchy areas of dense MNP layers that are probably pinned at the domain walls. The larger MNPs showed the most pronounced layering at the substrate surface, owing to their larger magnetic moment. The 5 nm MNPs show less pronounced layering as here – as of the smaller magnetic moment – Brownian motion is playing a more crucial role over the magnetic ordering by Néel relaxation. Still all self-assembled layers are well attached and stable against rinsing, sonication and even wiping.[18] With advancing

technology in the field of magnetic data storage, Henderson *et al.* demonstrated the use of commercial hard disk drive media for the self-assembly of 10 nm Fe_3O_4 MNPs from a ferrofluid. Furthermore, they transferred the resulting MNP patterns into a polymer film that can be peeled off the template. This results in a free-standing MNP pattern within the film, exemplified by the authors by the refraction of light (Figure 14.1f). As the template pattern can be digitally induced with ~10 nm spatial resolution by conventional hard disk drive data writing, this opens up an interesting way of high-resolution, large-area patterning of MNPs.[7]

14.3 2D-printed Structures

Two decades ago, the development of soft lithography and scanning probe lithography (SPL) tools introduced a new paradigm in the creation of 2D nanostructures, which was soon leveraged to organize MNPs in custom shapes for their integration into devices.[19] In comparison to physical synthesis methods,[20] which have proven to produce highly ordered NP arrays,[21] printing technologies brought additional flexibility in patterning and choice of NPs. In the following section, we focus on two 2D printing techniques with particular relevance in the field: microcontact printing (μCP) and dip-pen nanolithography (DPN).

14.3.1 Microcontact Printing

Amongst the family of soft lithography techniques, microcontact printing has often been used to produce structures of MNPs.[22–30] The technique was initially conceived as an elastomeric stamp [usually polydimethylsiloxane (PDMS)] for the transfer of molecular inks upon contact between the stamp and substrate, forming custom-shaped self-assembled monolayers.[31,32] Its development and extension to print different inks[33,34] led to a variety of applications that range from microelectronics, surface chemistry and cell biology. The very first publications related to MNP structuring with μCP were related to SA on pre-patterned substrates. Some pioneering work published in 1996 already showed 50–150 nm-big magnetite (Fe_3O_4) NPs forming micron-sized square patterns *via* selective wetting on pre-coated substrates.[23] By using PDMS stamps to pattern hydrophobic self-assembled thiol monolayers (hexadecanethiol) followed by incubation with hydrophilic nature thiols (*e.g.* 2-aminoethanethiol) to fill the bare substrate parts, two areas with different wettability properties were created. Dipping the prepared substrate on colloidal NP suspensions led to the formation of droplets in the hydrophilic areas upon drying of the samples.[22,23] The same work reports some results achieved using capillary filling,[23] a complementary strategy, where the substrate is covered with an elastomeric stamp,

while a droplet of colloidal NP ink flows to the grooves driven by capillary forces.[26]

Other indirect MNP patterning methods tackle the surface modification of designated substrate regions to create a template that selectively binds NPs through various interactions, such as covalent binding[27] or ligand exchange reactions[24,28] between the substrate and the NP surface terminal groups.

Conversely, on direct patterning techniques, NPs are adsorbed on microcontact printing stamps and then transferred to the desired substrate upon contact. Prior to magnetic NPs, gold NPs were transferred to the PDMS stamps through the Langmuir–Blodgett (LB) method.[35,36] MNPs can be transferred from the liquid–gas interface to the PDMS stamp during their immersion in an MNP colloidal suspension while controlling some suspension-related parameters, such as the surface pressure and pH or the substrate-lifting rate.[25,37–39] Park *et al*. optimized the LB parameters to obtain a homogeneous Co NP film forming a hexagonal closely packed structure on the stamps that were then carefully micropatterned on an electronic circuit and achieved ohmic conductivity after annealing with similar resistance values to others reported previously.[40]

A variation of this technique, termed overpressure contact printing (oCP), was used to pattern FePt magnetic rings by adsorbing Pt@Fe_2O_3 NPs through the LB method and transferring them to the substrate, leveraging the deformation of low aspect-ratio feature elastomeric stamps.[29] The subsequent annealing treatment for the reduction of the core–shell NPs[25,38] yielded FePt alloy structures grown in a tetragonal phase, which were later studied with magnetic force microscopy (MFM) imaging. Due to the soft magnetic nature of FePt, all cases revealed attractive interaction between the MFM tip and the fabricated structures.[25,29,38]

Ding *et al*. discuss the convenience of using hydrophobic PDMS stamps, which not only avoid exposure to an oxygen plasma procedure to render the stamp hydrophilic but also improve the transfer of NPs to the desired substrate due to the low affinity between the PDMS stamp and the nanoparticle surface.[30] In their work, Fe_2O_3 NPs are patterned and used as a catalyser to grow carbon nanotubes through chemical vapour deposition (CVD), concluding that higher MNP concentration promotes agglomerations and leads to less efficient catalysis. An alternative approach to improve NP adhesion on substrates was presented by Kinge *et al*.,[41] where click chemistry reactions between alkyne-functionalized FePt NPs and amide-terminated self-assembled monolayers (SAMs) on silicon oxide resulted in irreversible attachment of the NPs to the surface *via* triazole linkers.

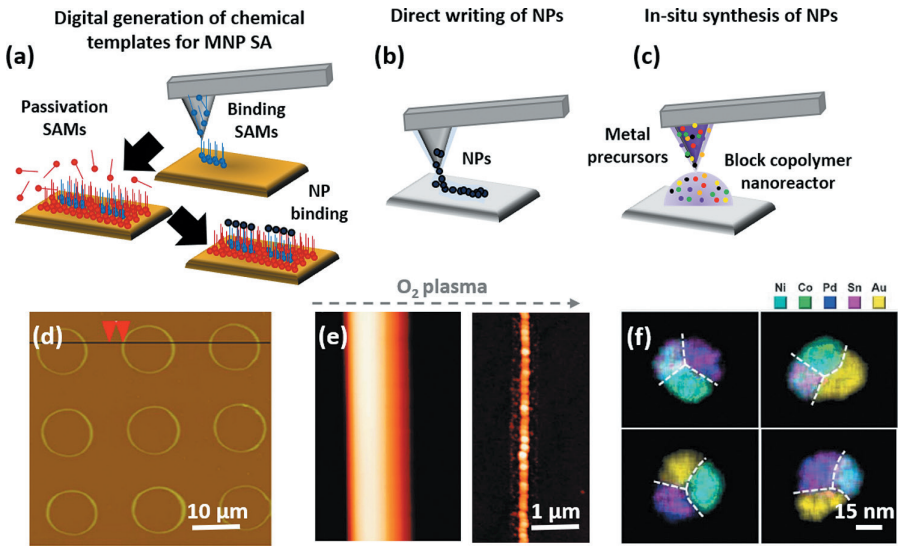

Figure 14.2 (a), (b) and (c) Scheme of different approaches to MNP writing *via* DPN. (d) AFM image of nanorings made *via* dewetting of a polymer-coated MNP solution on patterned self-assembled monolayers. (e) Direct-written MNP line, before and after O_2 plasma exposure. (f) Polyelemental MNPs synthesized through SPBCL. (d) Reproduced from ref. 22 with permission from Elsevier, Copyright 2005; (e) adapted from ref. 48 with permission from American Chemical Society, Copyright 2010; (f) reproduced from ref. 49 with permission from AAAS, Copyright 2019.

14.3.2 Dip-pen Nanolithography

In 1999, Mirkin *et al.* introduced a new SPL tool called dip-pen nanolithography, where an atomic force microscopy (AFM) probe was used as a quill-pen to transfer thiol molecules to a gold substrate, forming self-assembled monolayers.[42] In the following decade, the capabilities of DPN quickly expanded to structure/pattern different types of species from biomolecules[43] to metal ions,[44] sols,[45] polymers[46] or NPs,[47] many of which were developed by Mirkin *et al.* themselves.

Different approaches were developed to achieve controlled patterning of MNPs, which can be grouped into three main categories, related to the driving physical/chemical phenomena behind, as summarized in Figure 14.2: (1) digital generation of chemical templates, (2) direct writing of MNPs and (3) *in-situ* synthesis of MNPs.

14.3.2.1 Digital Generation of Chemical Templates for MNP SA

The capability to pattern SAMs on substrates was soon leveraged to immobilize different species through chemical binding on templates

generated by DPN (Figure 14.2a).[50] Fe_3O_4 and $MnFe_2O_4$ MNPs were used with a tetramethylammonium hydroxide coating, which served as a surfactant to avoid MNP agglomeration and increased their affinity for the negatively charged 16-mercaptohexadecanoic acid (MHA) pre-patterned on the surface.[50] A similar strategy was followed by Wang *et al.*[51] to pattern carbon-coated sub-5 nm Fe MNPs, with improved magnetic properties (higher blocking temperature and coercivity) compared to their Fe_3O_4 counterparts. The NPs were dispersed in a 1,2-dichlorobenzene solution, which only wets the hydrophilic regions, *i.e.* MHA, making the MNPs flow and immobilize exclusively on the DPN pre-patterned parts. They correlated the size of the MHA patterns with the number of MNPs deposited and proved that MNPs can be individually lined up (Figure 14.2b).[51]

Other examples of chemical template generation through DPN include the use of biomolecular conjugation with inorganic NPs.[52,53] Polymeric patterns of poly(sodium-4-styrenesulfonate) (PSS) can be created with DPN and used to immobilize DNA molecules that have been coupled to the Fe_3O_4 NP surface in a site-specific manner.[52] Pre-patterning has also been conducted by other SPL methods, such as local anodization,[53,54] to obtain carboxylic acid-terminated patterns on C_{18} monolayer-functionalized Si surfaces.[54] This is followed by two steps, such as covalent linking of tyramine to the generated carboxylic acid end-groups and subsequent tyrosinase-induced conversion of the hydroxyphenyl end-group into a catechol, which act as specific binding sites for Fe_3O_4 NPs linked through surface Fe^{3+} ions.

14.3.2.2 Direct Writing of MNPs

After the direct patterning of molecules, the extension of this method to other species, such as the direct delivery of NPs from the AFM tip to a desired substrate (Figure 14.2b), constituted the next milestone.[47,55] This is, however, not a diffusive process and requires the presence of a surfactant to keep the NP ink in a liquid-like state or alternatively a polymer matrix to enable the flow of the ink. Citrate-capped g-Fe_2O_3 nanocrystals of 11 nm prepared by wet-chemical means were successfully patterned, after immersing the AFM probes in a dispersion for 5–10 min followed by drying, and studied by magnetic imaging techniques.[56] A similar approach was followed by Roy *et al.*, who patterned citrate-capped $CoFe_2O_4$ additionally to CdSe/ZnS core–shell quantum dots and proved their optical and magnetic functionality.[57]

Long-chain ligands, such as trioctylphosphine oxide (TOPO) and oleic acid, are used due to their capability to trap solvent molecules and keep the inks in a liquid-like state to achieve MNP printability and used as catalysts to grow single-walled carbon nanotubes (SWCNT) with controlled alignment on ST-cut quartz.[58]

Inorganic NPs can mix well with many polymers due to the adhesion of their side chains to the hydroxyl groups of their external native oxide

layer. Several authors have leveraged this property to produce a polymer–NP ink that can controllably flow from tip to surface.[48,59,60] Lee *et al*. deposited different NPs, ranging from Au, Ag or Fe_3O_4, on a poly(methyl methacrylate) (PMMA) matrix, which were from a heated AFM probe.[48] The exposure to oxygen plasma of the patterned composite lines leads to an alignment of the NPs (Figure 14.2e), which, according to the authors, is driven by a polymer matrix shearing mechanism during deposition. Interestingly, the degree of alignment can be improved by (1) enhancing the NP coating–polymer interaction or (2) local viscosity of the composite.

In turn, Mirkin *et al.* proposed the encapsulation of NPs within a polyethylene glycol (PEG) matrix as a way to achieve control over patterning feature diameters with the dwell time, independently on the chosen surface or NPs.[59] Kandemir *et al*. went one step further and explored the conditions to achieve polymer composites with evenly distributed $CoFe_2O_4$ and $BaTiO_3$ NPs. They also shed light on the importance of the ink volume, physisorption and surface diffusion in the patterning process by studying cross-sectional SEM imaging of focused ion beam (FIB)-milled patterns.[60]

14.3.2.3 *In-situ* Synthesis of MNPs

In 2003, Mirkin *et al.* proposed a local sol–gel-based method combined with DPN, where a BaFe precursor in ethylene glycol solution was used to generate sub-100 nm resolution patterns, which were subsequently annealed to create barium ferrite features. Similarly, Shin *et al*. fabricated arbitrary-shaped magnetic nanopatterns using an AFM probe coated with an iron nitrate $Fe(NO_3)_3{\cdot}9H_2O$ solution and studied the magnetic domain configurations of the formed Fe_2O_3 structures with MFM.[61] Amongst the *in-situ* NP synthesis techniques, the scanning probe block copolymer lithography (SPBCL) deserves some special mention.[62] Attoliter volume block co-polymer nanoreactors (poly(ethylene oxide)-*b*-poly(2-vinylpyridine)) concentrate nanomaterial precursors to later create individual NPs with great spatial control, achieving diverse structural and chemical features. After the first publication in 2010, a polyelemental NP library creation followed in 2016, showing control over composition and size independently for a combination of five metallic elements (Au, Ag, Co, Cu and Ni) through the polymer nanoreactor-mediated synthesis.[63] A last contribution to this research line was recently published, and particle libraries were extended to the preparation of NPs with seven elements and four phases with complex tailored interfacial chemistries (Figure 14.2f).[49]

14.4 3D Printing of Magnetic Microstructures

The emergence of new 3D printing technologies together with the development of miniaturization techniques holds promise to start a new industrial and technological era through the incorporation of

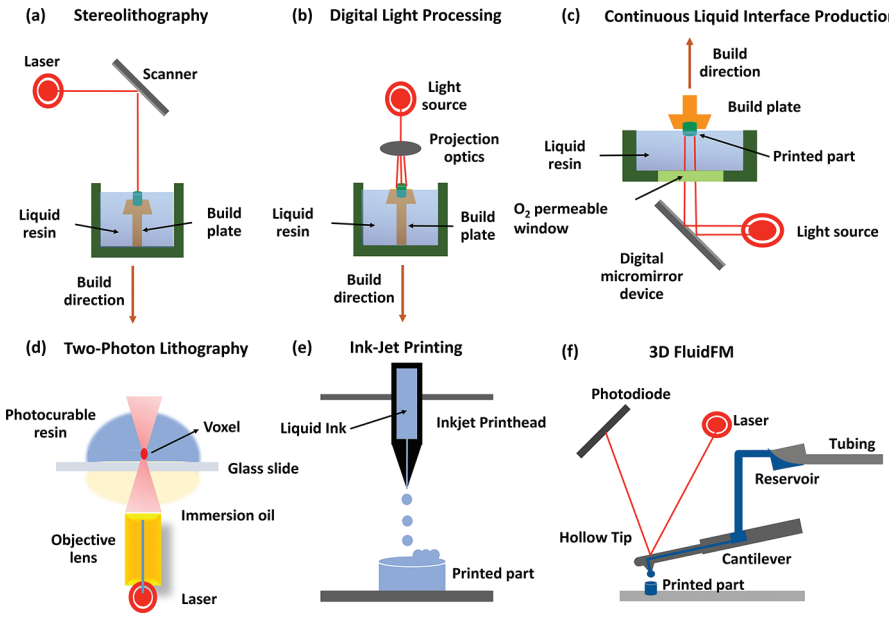

Figure 14.3 Schematics of 3D printing methods relevant for printing magnetic microstructures: (a) Stereolithography (SLA), (b) digital light processing (DLP), (c) two-photon lithography (2PL), (d) continuous liquid interface production (CLIP), (e) inkjet printing (IJP) and (f) FluidFM.

complex-shaped multifunctional microstructures.[64–66] From the Internet-of-things (IoF) environments[67,68] to the integration of theranostic *in-vivo* devices,[69] many technological fields will benefit from the development of stimuli-responsive microstructures. In particular, the capability to respond to external magnetic fields possesses some inherent advantages in comparison to other stimuli (thermal, chemical, electrical, *etc.*), such as the possibility for remote control or high controllability.[68] Towards this aim, MNPs incorporated as active elements to polymeric matrices play a central role.[69–74] Despite the rapid development of 3D printing of magnetoresponsive materials on the macroscale, fabrication of micron-sized structures (resolution below 100 μm) is still an emerging field, which will be the focus of this part of the chapter. Amongst the different technologies available for 3D printing, most of the published research has been tackled through the family of vat polymerization (VP) techniques, which comprises several techniques, such as stereolithography (SLA),[75,76] digital light processing (DLP),[77] continuous liquid interface production (CLIP)[74] and two-photon lithography (2PL)[69,78–80] (see Figure 14.3). Work related to inkjet printing (IJP) with MNPs[66,81–84] or extrusion-based 3D printing[85] can be found, although the 3D printing capabilities of this have not yet been

explored or aimed at bigger structures. In the following section, we describe the techniques to fabricate 3D magnetic microstructures and describe some examples.

14.4.1 VP Techniques

In vat polymerization techniques, radiation selectively polymerizes liquid-photosensitive resins in a vat to form 3D structures. Amongst the most widespread, SLA is an additive manufacturing process[86] that uses a ultraviolet (UV) laser to subsequently cure layers of liquid resin into the desired shape. The laser beam traces out the cross-section of the object being printed, curing the resin into a solid form (Figure 14.3a). The platform then lowers by a small increment, and the process is repeated, building up the entire structure layer by layer. The incorporation of NPs into the photopolymer has frequently been exploited to build macroscopic structures.[65,87,88] Few reports address the fabrication of SLA-built magnetoresponsive structures with sub-100 μm resolution. Martin *et al*. developed the idea of magnetic-field-assisted 3D printing through SLA.[76] In their work, dense ceramic/polymer composites were printed, with embedded micrometre-sized alumina particles and electrostatically adsorbed iron oxide NPs on their surface. A magnetic field is coupled to the SLA platform enabling specific alignments of functional fillers, greatly increasing strength, stiffness and toughness. Selective curing of desired parts of the resin while changing the magnetic field orientation allows the integrating of parts with custom mechanical robustness. Such magnetically aligned composite proved to be advantageous for biomedical applications in terms of mechanical reinforcement; thus, the same concept was used to fabricate bioinspired painless microneedles (MNs).[75] The assembly of magnetic iron oxide particles during printing into a hierarchical structure allowed to build a robust microneedle, taking inspiration from a limpet tooth. Magnetic field intensity, MNP size and concentration in printable composites affect the mechanical reinforcement of magnetic field-assisted 3D-printed MNs.

In DLP, a digital light projector is used to cure a photopolymer resin by illuminating it with a 2D pixel pattern (Figure 14.3b). Zhu *et al*. reported a higher-resolution variant of this technique, coined microscale continuous optical printing (μCOP), and used it to print hydrogel-based [poly(ethylene glycol) diacrylate (PEGDA), a biocompatible hydrogel] swimming microfish structures with detoxification capability. The selective incorporation of MNPs endowed different functionalities: catalytic Pt NPs propel the microfish through H_2O_2 decomposition and Fe_2O_3 NPs direct its movement.[73] One of the most promising 3D printing techniques in terms of fabrication speed, CLIP[89] deserves some mention, as it is still in development and authors recently reported significant improvement in its resolution.[90] It sequences UV images that are projected through an oxygen-permeable, UV-transparent window beneath a liquid resin bath using a

digital light processing imaging unit. To maintain a liquid interface below the advancing part, a dead zone above the window is created, while a constant suction force continuously renews the reactive liquid resin above the dead zone (Figure 14.3d). Shao *et al.* addressed the problem of the incorporation of higher amounts of NPs into the resin for a bigger magnetic response through this technique and achieved (30 wt% solid loading of Fe_2O_3 NPs) overcoming the problems related to ink viscosity and lower polymerization rates.[74]

In terms of resolution, two-photon lithography (2PL) is the best candidate amongst the aforementioned techniques, as a number of applications, including nano-sensing and nano-electronics or biological applications at a single-cell scale, require sub-micrometre-resolution features. 2PL involves the polymerization of a photosensitive material (a blend of a radical-generating component or photoinitiator and a bulk of unsaturated monomers) by means of a focused pulsed laser, almost 100 nm resolution.[91] The high density of photons at the laser focal spot induces the simultaneous absorption of two photons by the photoinitiator molecules to start a radical polymerization reaction, which remains confined in the focal spot volume, called voxel. By moving the photoresist relative to the focal spot, it is possible to compose lines in three dimensions and, in turn, 3D microstructures of significant complexity (see Figure 14.3c). Despite the palette of applications covered by 2PL structures, including scaffolds for cell biology,[92–94] metamaterials,[95,96] micro-optics[97] and micro- and nano-actuators,[98] the number of magnetically driven devices realized *via* 2PL referred in the literature is relatively low,[78,99] and the main approach used to build magnetic micro-devices still consists of post-processing 2PL polymeric scaffolds *via* physical vapour deposition (PVD) of magnetic alloys.[100–104] However, the use of PVD methods hinders the realization of complex geometries due to shadowing of parts of the structures on the other areas of the same device, and selective functionalization is also missing.[105] An alternative deposition strategy was proposed by Dong *et al.*, requiring the physisorption of magnetic NPs in water, which led to a uniform magnetic layer.[106] A more complex method was developed *via* electroless deposition of an Ni-based layer[107,108]: through immersion of a sample in a solution containing metal ions, a complexing agent and a reductant. A redox reaction results in the homogeneous deposition of a metallic layer on the structure.

The used photoresist can also include a number of other chemicals, *e.g.* co-monomers,[98] reactive molecules for post-polymerization processing,[109,110] thickeners,[111] organic–inorganic monomers[112] and MNPs. The first examples of monomer/magnetic material mixtures were proposed by Sun *et al.* a decade ago,[80,113] who fabricated a microturbine with a mixture of acrylate monomers and Fe_3O_4 NPs. The microdevice was realized inside a microfluidic channel and was capable of rotatingaround a central shaft. The same principle was exploited to realize swimmers similar to the ones previously

described.[114] In particular, a mixture of methacrylated chitosan, a suitable photoinitiator and MNPs was polymerized *via* 2PL in a helicoidal shape, and its remotely controlled motion in liquid was demonstrated. Researchers also exploited the capability of chitosan to be degraded enzymatically and release biomolecules (*i.e.* doxorubicin) in the surrounding environment. Indeed, they created a magnetic carrier of doxorubicin, which at once fulfilled the functions of (1) drug transporter and (2) drug deliverer. The same group further improved this approach proposing a multifunctional, theranostic device,[69] where anti-ErbB-2 antibody-tagged Fe_3O_4 NPs were magnetically driven to tumour-like environments *in vitro*. The abnormal concentration of matrix metalloproteinases (MMP2) induced the complete degradation of the swimmers, and MNPs were released to selectively target cells presenting the antigens to the anti-ErbB-2 antibody.

The major drawback of this approach is that the transparency of the ink is severely affected,[115] as even when the concentration of MNP is low, the transmittance of the laser radiation through the resists is strongly reduced, lowering the available photon density below the polymerization threshold.

A smart approach to circumvent the challenges posed by the opaqueness of magnetically loaded materials was suggested by Lee *et al.*,[116] which involves polymerizing the negative photoresist in arbitrary shapes and then inducing a surface functionalization reaction between structures and chemically modified magnetic NPs. This strategy was pursued, where aminated magnetic NPs were covalently bound to 2PL-fabricated microhelices made of aminated PEGDA, *via* 2-sulfo-NHS disulfide. The efficiency of this functionalization was demonstrated by migration tests in liquid under magnetic fields of 15–25 mT. Despite representing a significant advancement in the landscape of magnetically modified microstructures fabricated *via* 2PL, this technique is still not mature yet, as the functionalization must be carried out on the whole structure. As post-processing approaches to modify 2PL device surfaces are available, the strategies mentioned so far should converge towards a novel class of magnetically modified structures, where only those parts of the device that are functional for propulsion, swimming, deflection, *etc.*, can be decorated with magnetic NPs. This would strikingly increase the degree of freedom in the fabrication of arbitrarily complex 3D micro-machines.

14.4.2 Direct Writing and Other Approaches

A promising 3D printing method based on direct ink writing, namely IJP, is a non-contact method of additive manufacturing that has often been used to create 2D patterns. Using micrometre-sized printhead nozzles, the IJP process dispenses liquid-phase materials in a controlled manner. A thin layer of ink residue is formed when the liquid phase material, known as ink, is dispensed from droplets in a specified pattern onto a surface. Small-sized droplets and high positioning accuracy make IJP

ideal for 3D printing, whereby the 3D structure is created by layering new layers on top of one another (also called material jetting).[117,118] Despite its potential, not many reports can be found on the use of this technology to create magnetic microstructures. Jacot-Descombes *et al*. demonstrated that SU-8-based superparamagnetic NP (Fe_3O_4) polymer composite (SPMPC) microstructures can be fabricated *via* IJP followed by thermal curing.[82] An external magnetic field is used to obtain preferential magnetic directions composed of dense NP lines before thermally crosslinking the composite. A recent development of other direct-writing techniques based on SPL towards 3D printing, using either DPN[119,120] or FluidFM,[121–123] has been achieved. FluidFM is an SPL technique where a microsized closed-channel patterned inside an AFM cantilever dispenses an ink locally, while the applied force with the tip is controlled through a standard AFM laser detection system (Figure 14.3f). Similar to IJP, a UV-curable polymeric ink can be written layer-by-layer, until a sub-micron-resolution 3D prototype is created. So far, no magnetic functionality has been added to these 3D polymeric structures, although in the case of the FluidFM technology, purely metallic 3D structures (including magnetic alloys) have recently been achieved through electroplating at a micrometre scale.[124,125]

An entirely different approach consists of using pre-design templates, a technique particularly relevant to build magnetic actuated flexible

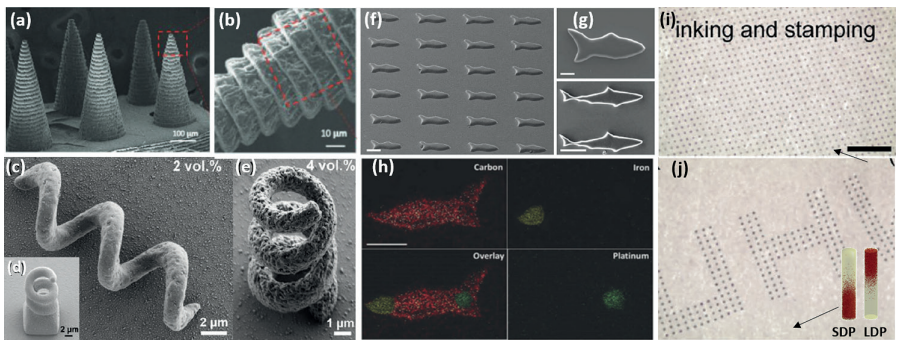

Figure 14.4 (a) Limpet tooth-inspired 3D-printed microneedle array with Fe_3O_4 fillers and (b) magnification of one of them.[75] Helical microrobots fabricated through 2PL with (c) and (d) 2% and (e) 4 vol% NP filling.[115] (f) and (g) PEGDA microfish body printed with functional Pt and Fe_3O_4 NPs shown in (h).[73] (i, j) Hybrid flexible micropillars with different magnetic responsivities depending on the NP location within the micropillar geometry.[70] Panels (a, b) Reproduced from ref. 75 with permission from John Wiley & Sons, Copyright © 2020 Wiley-VCH GmbH, (c–e) reproduced from ref. 115 with permission from Springer Nature, Copyright 2013, (f–h) reproduced from ref. 73 with permission from John Wiley & Sons, Copyright © 2015 WILEY-VCH Verlag GmbH & Co. KGaA, Weinheim, (i, j) reproduced from ref. 70 with permission from John Wiley & Sons, Copyright © 2020 WILEY-VCH Verlag GmbH & Co. KGaA, Weinheim.

micropillars, which allows creating smart surfaces with on-demand wettability properties[120–123] or controlled fluid behaviour and droplet/object manipulation. Despite the widespread use of microparticles for this type of actuation,[126–128] more sophisticated approaches rely on MNPs,[70–72] where downsizing the particle size makes control over the spatial distribution of MNPs within the polymeric matrix possible. Interestingly, selective covering of the desired micropillars while curing yields heterogeneous, bending actuations, as particles can be oriented in different directions during this process[70] (Figure 14.4i and j). This site-selective MNP distribution leads to selective bending and can be used for droplet transportation.[129] As UV-cured structures generally lack reprogrammability, Ni *et al.* have recently reported an original method, where they fabricated elastomeric hollow micropillars that were filled with liquid Fe_3O_4 NP-carrying resins, to allow the rearrangement of MNP distribution dynamically.[71] Different patterns were written after applying a global magnetic field to homogenize and leave all the pillars with the same NP distribution (or state) and then approaching a magnetic needle to selectively modify the state of some pillars, where the patterned structure will appear upon actuation.

14.5 Challenges and Future Directions

The combination of magnetic materials with high-resolution 3D printing technologies is significantly expanding the range of feasible devices and addressable scientific questions. Nevertheless, the integration of nanocomposites, and more specifically MNPs, into 3D elastomeric architectures is still very limited. Some of the challenges faced by the printing community are related to the resolution of the techniques, which will foreseeably improve in the coming years. The concentration of MNPs in most of the aforementioned examples is still limited, as the addition of nanoelements changes the light scattering in VP techniques, as well as changes in the rheological properties in direct ink printing techniques, such as IJP or FluidFM. Additionally, high MNP concentration can lead to aggregation problems. From this viewpoint, new ink formulations with enhanced magnetic performance need to be engineered. Therefore, we envisage that a joint interdisciplinary effort will be needed to alleviate these challenges and allocate the existing 3D printing technologies to build magnetoresponsive structures.

Acknowledgements

E.B. acknowledges the Karlsruhe Institute of Technology for a postdoctoral fellowship in the frame of the YIG Prep Pro program and the

Spanish Ministerio de Ciencia e Innovación (MICINN) through the Juan de la Cierva fellowhip IJC2020-044372-I funded by MCIN/AEI. This work was partly supported by the Karlsruhe Nano Micro Facility (KNMFi, www.knmf.kit.edu), a Helmholtz Research Infrastructure at Karlsruhe Institute of Technology (KIT, www.kit.edu).

References

1. S. Majidi, F. Z. Sehrig, S. M. Farkhani, M. S. Goloujeh and A. Akbarzadeh, Current methods for synthesis of magnetic nanoparticles, *Artif. Cells, Nanomed., Biotechnol.*, 2016, **44**, 722–734.
2. P. Tartaj, M. Del Puerto Morales, S. Veintemillas-Verdaguer, T. González-Carreño and C. J. Serna, The preparation of magnetic nanoparticles for applications in biomedicine, *J. Phys. D: Appl. Phys.*, 2003, **36**, R182–R197.
3. S. Wang, Z. Wang and Y. Hou, Self-assembled magnetic nanomaterials: Versatile theranostics nanoplatforms for cancer, *Aggregate*, 2021, **2**, 1–12.
4. E. V. Amadi and A. Venkataraman, Nanoscale self-assembly: concepts, applications and challenges, *Nanotechnology*, 2022, **33**, 185304.
5. J. B. Tracy and T. M. Crawford, Magnetic field-directed self-assembly of magnetic nanoparticles, *MRS Bull.*, 2013, **38**, 915–920.
6. X. Ye, *et al.*, Structural diversity in binary superlattices self-assembled from polymer-grafted nanocrystals, *Nat. Commun.*, 2015, **6**, 1–10.
7. J. Henderson, S. Shi, S. Cakmaktepe and T. M. Crawford, Pattern transfer nanomanufacturing using magnetic recording for programmed nanoparticle assembly, *Nanotechnology*, 2012, **23**, 185304.
8. T. Wen and S. A. Majetich, Ultra-large-area self-assembled monolayers of nanoparticles, *ACS Nano*, 2011, **5**, 8868–8876.
9. G. Singh, *et al.*, Self-assembly of magnetite nanocubes into helical superstructures, *Science*, 2014, **345**, 1149–1153.
10. C. Preger, M. Josefsson, R. Westerström and M. E. Messing, Bottom-up field-directed self-assembly of magnetic nanoparticles into ordered nano- and macrostructures, *Nanotechnology*, 2021, **32**, 195603.
11. K. Theis-Bröhl, *et al.*, Self-assembly of magnetic nanoparticles in ferrofluids on different templates investigated by neutron reflectometry, *Nanomaterials*, 2020, **10**, 1–15.
12. K. Theis-Bröhl, *et al.*, Self assembly of magnetic nanoparticles at silicon surfaces, *Soft Matter*, 2015, **11**, 4695–4704.
13. K. Theis-Bröhl, *et al.*, Self-Assembled Layering of Magnetic Nanoparticles in a Ferrofluid on Silicon Surfaces, *ACS Appl. Mater. Interfaces*, 2018, **10**, 5050–5060.
14. A. Saini, *et al.*, Magnetic Particle Self-Assembly at Functionalized Interfaces, *Langmuir*, 2021, **37**, 4064–4071.

15. G. Chen, *et al.*, Damascene process for controlled positioning of magnetic colloidal nanocrystals, *Adv. Mater.*, 2010, **22**, 1364–1368.
16. F. Bitter, On inhomogeneities in the magnetization of ferromagnetic materials, *Phys. Rev.*, 1931, **38**, 1903–1905.
17. St. Porthun, P. ten Berge and J. C. Lodder, Bitter colloid observations of magnetic structures in perpendicular magnetic recording media, *J. Magn. Magn. Mater.*, 1993, **123**, 199–208.
18. A. Saini, *et al.*, Layering of magnetic nanoparticles at amorphous magnetic templates with perpendicular anisotropy, *Soft Matter*, 2020, **16**, 7676–7684.
19. E. Bellido, N. Domingo, I. Ojea-Jiménez and D. Ruiz-Molina, Structuration and integration of magnetic nanoparticles on surfaces and devices, *Small*, 2012, **8**, 1465–1491.
20. M. Goiriena-Goikoetxea, A. García-Arribas, M. Rouco, A. V. Svalov and J. M. Barandiaran, High-yield fabrication of 60 nm Permalloy nanodiscs in well-defined magnetic vortex state for biomedical applications, *Nanotechnology*, 2016, **27**, 175302.
21. S. W. Lee, *et al.*, Highly sensitive biosensing using arrays of plasmonic Au nanodisks realized by nanoimprint lithography, *ACS Nano*, 2011, **5**, 897–904.
22. L. An, *et al.*, Patterned magnetic rings fabricated by dewetting of polymer-coated magnetite nanoparticles solution, *J. Colloid Interface Sci.*, 2005, **288**, 503–507.
23. S. Palacin, *et al.*, Patterned magnetic rings fabricated by dewetting of polymer-coated magnetite nanoparticles solution, *Chem. Mater.*, 1996, **8**, 1316–1325.
24. O. Yildirim, *et al.*, Monolayer-directed assembly and magnetic properties of FePt nanoparticles on patterned aluminum oxide, *Int. J. Mol. Sci.*, 2010, **11**, 1162–1179.
25. R. N. Patel, *et al.*, Printed magnetic FePt nanocrystal films, *ACS App. Mater. Interfaces*, 2009, **11**, 1339–1346.
26. M. Cavallini, *et al.*, Multiple-length-scale patterning of magnetic nanoparticles by stamp assisted deposition, *J. Phys.: Condens. Matter*, 2008, **20**, 204144.
27. S.-S. Bae, *et al.*, Selectively assembled Co nanoparticle stripes prepared by covalent linkage and microcontact printing, *J. Phys. Chem. B*, 2004, **108**, 2575–2579.
28. Y. Jie, *et al.*, Laterally patterned magnetic nanoparticles, *J. Mater. Chem.*, 2012, **22**, 1962–1968.
29. Q. Guo, X. Teng and H. Yang, Overpressure contact, *Nano Lett.*, 2004, **4**, 1657–1662.
30. L. Ding, *et al.*, Direct preparation and patterning of iron oxide nanoparticles via microcontact printing on silicon wafers for the growth of single-walled carbon nanotubes, *Chem. Mater.*, 2006, **18**, 4109–4114.

31. L. Yan, W. T. S. Huck, X. M. Zhao and G. M. Whitesides, Patterning Thin Films of Poly(ethylene imine) on a Reactive SAM Using Microcontact Printing, *Langmuir*, 1999, **15**, 1208–1214.
32. A. Perl, D. N. Reinhoudt and J. Huskens, Microcontact printing: Limitations and achievements, *Adv. Mater.*, 2009, **21**, 2257–2268.
33. T. Kaufmann and B. J. Ravoo, Stamps, inks and substrates: Polymers in microcontact printing, *Polym. Chem.*, 2010, **1**, 371–387.
34. S. Alom Ruiz and C. S. Chen, Microcontact printing: A tool to pattern, *Soft Matter*, 2007, **3**, 168–177.
35. V. Santhanam and R. P. Andres, Microcontact Printing of Uniform Nanoparticle Arrays, *Nano Lett.*, 2004, **4**, 41–44.
36. V. Santhanam, J. Liu, R. Agarwal and R. P. Andres, Self-assembly of uniform monolayer arrays of nanoparticles, *Langmuir*, 2003, **19**, 7881–7887.
37. Q. Guo, X. Teng, S. Rahman and H. Yang, Patterned Langmuir - Blodgett films of monodisperse nanoparticles of iron oxide using soft lithography, *J. Am. Chem. Soc.*, 2003, **125**, 630–631.
38. Q. Guo, X. Teng and H. Yang, Fabrication of magnetic FePt patterns from Langmuir-Blodgett films of platinum-iron oxide core-shell nanoparticles, *Adv. Mater.*, 2004, **16**, 1337–1341.
39. C. T. Black, C. B. Murray, R. L. Sandstrom and S. Shouheng, Spin-Dependent Tunneling in Self -Assembled Cobalt Nanocrystal Superlattices, *Science*, 2000, **290**, 1131–1134.
40. J. II. Park, *et al.*, Langmuir monolayers of co nanoparticles and their patterning by microcontact printing, *J. Phys. Chem. B*, 2005, **109**, 13119–13123.
41. S. Kinge, T. Gang, W. J. M. Naber, W. G. van der Wiel and D. N. Reinhoudt, Magnetic nanoparticle assembly on surfaces using click chemistry, *Langmuir*, 2011, **27**, 570–574.
42. R. D. Piner, J. Zhu, F. Xu, S. Hong and C. A. Mirkin, Dip-Pen' nanolithography, *Science*, 1999, **283**, 661–663.
43. S. Lenhert, P. Sun, Y. Wang, H. Fuchs and C. A. Mirkin, Massively parallel dip-pen nanolithography of heterogeneous supported phospholipid multilayer patterns, *Small*, 2007, **3**, 71–75.
44. L. Basabe-Desmonts, *et al.*, Fabrication and visualization of metal-ion patterns on glass by dip-pen nanolithography, *Chemphyschem*, 2008, **9**, 1680–1687.
45. L. Fu, X. Liu, Y. Zhang, V. P. Dravid and C. A. Mirkin, Nanopatterning of 'hard' magnetic nanostructures via dip-pen nanolithography and a sol-based ink, *Nano Lett.*, 2003, **3**, 757–760.
46. B. W. Maynor, S. F. Filocamo, M. W. Grinstaff and J. Liu, Direct-writing of polymer nanostructures: Poly(thiophene) nanowires on semiconducting and insulating surfaces, *J. Am. Chem. Soc.*, 2002, **124**, 522–523.

47. W. M. Wang, R. M. Stoltenberg, S. Liu and Z. Bao, Direct patterning of gold nanoparticles using dip-pen nanolithography, *ACS Nano*, 2008, **2**, 2135–2142.
48. W. K. Lee, Z. Dai, W. P. King and P. E. Sheehan, Maskless nanoscale writing of nanoparticle-polymer composites and nanoparticle assemblies using thermal nanoprobes, *Nano Lett.*, 2010, **10**, 129–133.
49. P.-C. Chen, *et al.*, Interface and heterostructure design in polyelemental nanoparticles, *Science*, 2019, **363**, 959–964.
50. X. Liu, L. Fu, S. Hong, V. P. Dravid and C. A. Mirkin, Arrays of magnetic nanoparticles patterned via 'dip-pen' nanolithography, *Adv. Mater.*, 2002, **14**, 231–234.
51. Y. Wang, *et al.*, Superparamagnetic sub-5 nm Fe@C nanoparticles: Isolation, structure, magnetic properties, and directed assembly, *Nano Lett.*, 2008, **8**, 3761–3765.
52. D. Nyamjav and A. Ivanisevic, Templates for DNA-templated Fe3O4 nanoparticles, *Biomaterials*, 2005, **26**, 2749–2757.
53. B. Basnar, J. Xu, D. Li and I. Willner, Encoded and enzyme-activated nanolithography of gold and magnetic nanoparticles on silicon, *Langmuir*, 2007, **23**, 2293–2296.
54. S. Hoeppener, A. Susha, A. Rogach, J. Feldmann and U. Schubert, Guided Self-Assembly of Fe3O4 Nanoparticles on Chemically Active Surface Templates Generated by Electro-Oxidative Nanolithography, *Curr. Nanosci.*, 2006, **2**, 135–141.
55. M. Ben Ali, T. Ondarçuhu, M. Brust and C. Joachim, Atomic Force Microscope Tip Nanoprinting of Gold Nanoclusters, *Langmuir*, 2002, **18**, 872–876.
56. G. Gundiah, *et al.*, Dip-pen nanolithography with magnetic Fe2O3 nanocrystals, *Appl. Phys. Lett.*, 2004, **84**, 5341–5343.
57. D. Roy, *et al.*, Directly writing with nanoparticles at the nanoscale using dip-pen nanolithography, *Appl.Surf. Sci.*, 2007, **254**, 1394–1398.
58. B. Li, *et al.*, Patterning colloidal metal nanoparticles for controlled growth of carbon nanotubes, *Adv. Mater.*, 2008, **20**, 4873–4878.
59. L. Huang, *et al.*, Matrix-assisted dip-pen nanolithography and polymer pen lithography, *Small*, 2010, **6**, 1077–1081.
60. A. C. Kandemir, D. Erdem, H. Ma, A. Reiser and R. Spolenak, Polymer nanocomposite patterning by dip-pen nanolithography, *Nanotechnology*, 2016, **27**, 135303.
61. H. W. Shin and J. Y. Son, Ferromagnetic Fe_2O_3 nanopatterns prepared using dip-pen lithography, *Solid State Commun.*, 2018, **282**, 1–4.
62. J. Chai, *et al.*, Scanning probe block copolymer lithography, *Proc. Natl. Acad. Sci. U. S. A.*, 2010, **107**, 20202–20206.
63. P.-C. Chen, *et al.*, Polyelemental nanoparticle libraries, *Science*, 2016, **352**, 0–5.
64. Y. Zhu, *et al.*, 3D printing biomimetic materials and structures for biomedical applications, *Bio-Des. Manuf.*, 2021, **4**, 405–428.

65. C. Credi, *et al.*, 3D Printing of Cantilever-Type Microstructures by Stereolithography of Ferromagnetic Photopolymers, *ACS Appl. Mater. Interfaces*, 2016, **8**, 26332–26342.
66. H. Song, *et al.*, Inkjet printing of magnetic materials with aligned anisotropy, *J. Appl. Phys.*, 2014, **115**, 17E308.
67. Z. Lei, *et al.*, Traditional Dough in the Era of Internet of Things: Edible, Renewable, and Reconfigurable Skin-Like Iontronics, *Adv. Funct. Mater.*, 2020, **30**, 1908018.
68. K. J. Merazzo, *et al.*, Magnetic materials: A journey from finding north to an exciting printed future, *Mater. Horiz.*, 2021, **8**, 2654–2684.
69. H. Ceylan, *et al.*, 3D-Printed Biodegradable Microswimmer for Theranostic Cargo Delivery and Release, *ACS Nano*, 2019, **13**, 3353–3362.
70. Z. Wang, *et al.*, Hybrid Magnetic Micropillar Arrays for Programmable Actuation, *Adv. Mater.*, 2020, **32**, 1–11.
71. K. Ni, *et al.*, Core-Shell Magnetic Micropillars for Reprogrammable Actuation, *ACS Nano*, 2021, **15**, 4747–4758.
72. D. Tian, *et al.*, Fast Responsive and Controllable Liquid Transport on a Magnetic Fluid/Nanoarray Composite Interface, *ACS Nano*, 2016, **10**, 6220–6226.
73. W. Zhu, *et al.*, 3D-Printed Artificial Microfish, *Adv. Mater.*, 2015, **27**, 4411–4417.
74. G. Shao, H. O. T. Ware, L. Li and C. Sun, Rapid 3D Printing Magnetically Active Microstructures with High Solid Loading, *Adv. Eng. Mater.*, 2020, **22**, 1900911.
75. X. Li, *et al.*, Limpet Tooth-Inspired Painless Microneedles Fabricated by Magnetic Field-Assisted 3D Printing, *Adv. Funct. Mater.*, 2021, **31**, 1–11.
76. J. J. Martin, B. E. Fiore and R. M. Erb, Designing bioinspired composite reinforcement architectures via 3D magnetic printing, *Nat. Commun.*, 2015, **6**, 1–7.
77. S. Lantean, *et al.*, 3D Printing of Magnetoresponsive Polymeric Materials with Tunable Mechanical and Magnetic Properties by Digital Light Processing, *Adv. Materi. Technol.*, 2019, **4**, 1900505.
78. Y. Lin and J. Xu, Microstructures Fabricated by Two-Photon Polymerization and Their Remote Manipulation Techniques: Toward 3D Printing of Micromachines, *Adv. Opt. Mater.*, 2018, **6**, 1701359.
79. A. Servant, F. Qiu, M. Mazza, K. Kostarelos and B. J. Nelson, Controlled in vivo swimming of a swarm of bacteria-like microrobotic flagella, *Adv. Mater.*, 2015, **27**, 2981–2988.
80. Y. Tian, *et al.*, High performance magnetically controllable microturbines, *Lab Chip*, 2010, **10**, 2902–2905.
81. M. Cannamela, J. Stasiak, P. Harmon, T. Allen and P. Dhagat, Fabrication of Magnetic Polymer Nanocomposites Using Inkjet 3D Print Technology, *NIP Digital Fabr. Conf.*, 2020, **36**, 1–5.

82. L. Jacot-Descombes, *et al.*, Inkjet printing of high aspect ratio superparamagnetic SU-8 microstructures with preferential magnetic directions, *Micromachines*, 2014, **5**, 583–593.
83. P. Tiberto, *et al.*, Magnetic properties of jet-printer inks containing dispersed magnetite nanoparticles, *Eur. Phys. J. B*, 2013, **86**, 2–7.
84. D. S. Kolchanov, *et al.*, Sol–gel magnetite inks for inkjet printing, *J. Mater. Chem. C*, 2019, **7**, 6426–6432.
85. A. Hodaei, *et al.*, Single Additive Enables 3D Printing of Highly Loaded Iron Oxide Suspensions, *ACS Appl. Mater. Interfaces*, 2018, **10**, 9873–9881.
86. J. Z. Manapat, Q. Chen, P. Ye and R. C. Advincula, 3D Printing of Polymer Nanocomposites via Stereolithography, *Macromol. Mater. Eng.*, 2017, **302**, 1–13.
87. R. De Santis, *et al.*, 3D fibre deposition and stereolithography techniques for the design of multifunctional nanocomposite magnetic scaffolds, *J. Mater. Sci. Mater. Med.*, 2015, **26**, 1–9.
88. S. J. Leigh, *et al.*, A miniature flow sensor fabricated by micro-stereolithography employing A magnetite/acrylic nanocomposite resin, *Sens. Actuators, A*, 2011, **168**, 66–71.
89. G. Lipkowitz, *et al.*, Continuous liquid interface production of 3D objects, *Science*, 2015, **347**, 1349–1352.
90. K. Hsiao, *et al.*, Single-digit-micrometer-resolution continuous liquid interface production, *Sci. Adv.*, 2022, **8**, 46.
91. J. Fischer and M. Wegener, Three - dimensional optical laser lithography beyond the diffraction limit, *Laser Photonics Rev.*, 2013, **7**, 22–44.
92. M. Hippler, *et al.*, 3D Scaffolds to Study Basic Cell Biology, *Adv. Mater.*, 2019, **31**, e1808110.
93. K. Weißenbruch, E. D. Lemma, M. Hippler and M. Bastmeyer, Microscaffolds as synthetic cell niches: recent advances and challenges, *Curr. Opin. Biotechnol.*, 2022, **73**, 290–299.
94. N. Barin, *et al.*, 3D-Engineered Scaffolds to Study Microtubes and Localization of Epidermal Growth Factor Receptor in Patient-Derived Glioma Cells, *Small*, 2022, **18**, 2204485.
95. T. Frenzel, M. Kadic and M. Wegener, Three-dimensional mechanical metamaterials with a twist, *Science*, 2017, **358**, 1072–1074.
96. A. Münchinger, L.-Y. Hsu, F. Fürniß, E. Blasco and M. Wegener, 3D optomechanical metamaterials, *Mater. Today*, 2022, **59**, 9–27.
97. D. Gonzalez-Hernandez, *et al.*, Laser 3D printing of inorganic freeform micro-optics, *Photonics*, 2021, **8**, 1–12.
98. M. Hippler, *et al.*, Mechanical stimulation of single cells by reversible host-guest interactions in 3D microscaffolds, *Sci. Adv.*, 2020, **6**, eabc2648.
99. J. Li and M. Pumera, 3D printing of functional microrobots, *Chem. Soc. Rev.*, 2021, **50**, 2794–2838.

100. S. Tottori, *et al.*, Magnetic helical micromachines: fabrication, controlled swimming, and cargo transport, *Adv. Mater.*, 2012, **24**, 811–816.
101. F. Qiu, *et al.*, Magnetic Helical Microswimmers Functionalized with Lipoplexes for Targeted Gene Delivery, *Adv. Funct. Mater.*, 2015, **25**, 1666–1671.
102. R. Mhanna, *et al.*, Artificial bacterial flagella for remote-controlled targeted single-cell drug delivery, *Small*, 2014, **10**, 1953–1957.
103. X. Wang, *et al.*, Surface-Chemistry-Mediated Control of Individual Magnetic Helical Microswimmers in a Swarm, *ACS Nano*, 2018, **12**, 6210–6217.
104. X. Wang, *et al.*, MOFBOTS: Metal–Organic-Framework-Based Biomedical Microrobots, *Adv. Mater.*, 2019, **31**, 2–8.
105. A. Paris, D. Decanini and G. Hwang, Swimming force characterizations of multistaged bi-helical microswimmer and 3D vortex trap manipulation, *Microelectron. Eng.*, 2021, **235**, 111466.
106. M. Dong, *et al.*, 3D-Printed Soft Magnetoelectric Microswimmers for Delivery and Differentiation of Neuron-Like Cells, *Adv. Funct. Mater.*, 2020, **30**, 1910323.
107. P. Pip, *et al.*, Electroless Deposition of Ni-Fe Alloys on Scaffolds for 3D Nanomagnetism, *Small*, 2020, **16**, 1–7.
108. W.-K. Wang, *et al.*, Magnetic nickel-phosphorus/polymer composite and remotely driven three-dimensional micromachine fabricated by nanoplating and two-photon polymerization, *J. Phys. Chem. C*, 2011, **115**, 11275–11281.
109. R. Batchelor, *et al.*, Two in One: Light as a Tool for 3D Printing and Erasing at the Microscale, *Adv. Mater.*, 2019, **31**(40), 1904085.
110. B. Richter, *et al.*, Guiding Cell Attachment in 3D Microscaffolds Selectively Functionalized with Two Distinct Adhesion Proteins, *Adv. Mater.*, 2017, **29**, 1604342.
111. E. Scarpa, *et al.*, Microfabrication of pH-responsive 3D hydrogel structures via two-photon polymerization of high-molecular-weight poly(ethylene glycol) diacrylates, *Sens. Actuators, B*, 2019, **279**, 418–426.
112. A. Trautmann, M. Rüth, H. D. Lemke, T. Walther and R. Hellmann, Two-photon polymerization based large scaffolds for adhesion and proliferation studies of human primary fibroblasts, *Opt. Laser Technol.*, 2018, **106**, 474–480.
113. H. Xia, *et al.*, Ferrofluids for fabrication of remotely controllable micro-nanomachines by two-photon polymerization, *Adv. Mater.*, 2010, **22**, 3204–3207.
114. U. Bozuyuk, *et al.*, Light-Triggered Drug Release from 3D-Printed Magnetic Chitosan Microswimmers, *ACS Nano*, 2018, **12**, 9617–9625.
115. M. Suter, *et al.*, Superparamagnetic microrobots: Fabrication by two-photon polymerization and biocompatibility, *Biomed. Microdevices*, 2013, **15**, 997–1003.

116. H. Lee, D. Kim, S. Kwon and S. Park, Magnetically Actuated Drug Delivery Helical Microrobot with Magnetic Nanoparticle Retrieval Ability, *ACS Appl. Mater. Interfaces*, 2021, **13**, 19633–19647.
117. B. Elder, *et al.*, Nanomaterial Patterning in 3D Printing, *Adv. Mater.*, 2020, **32**(17), 1907142.
118. N. W. S. Pinargote, A. Smirnov, N. Peretyagin, A. Seleznev and P. Peretyagin, Direct ink writing technology (3D printing) of graphene-based ceramic nanocomposites: A review, *Nanomaterials*, 2020, **10**, 1–48.
119. G. Liu, *et al.*, 3D Dip-Pen Nanolithography, *Adv. Mater. Technol.*, 2022, **7**(8), 2101493.
120. E. Berganza, *et al.*, 3D Nanolithography by Means of Lipid Ink Spreading Inhibition, *Small*, 2023, **19**(10), 2205590.
121. J. Ventrici de Souza, *et al.*, Three-Dimensional Nanoprinting via Direct Delivery, *J. Phys. Chem. B*, 2018, **122**, 956–962.
122. T. G. Pattison, S. Wang, R. D. Miller, G. Liu and G. G. Qiao, 3D nanoprinting via spatially controlled assembly and polymerization, *Nat. Commun.*, 2022, **13**, 1–7.
123. E. Berganza, G. Apte, S. K. Vasantham and T. Nguyen, Integration of Biofunctional Molecules into 3D-Printed, *Polymers*, 2022, **14**, 1327.
124. C. Shen, *et al.*, Electrochemical 3D printing of Ni–Mn and Ni–Co alloy with FluidFM, *Nanotechnology*, 2022, **33**, 265301.
125. J. Hengsteler, *et al.*, Bringing Electrochemical Three-Dimensional Printing to the Nanoscale, *Nano Lett.*, 2021, **21**, 9093–9101.
126. M. Cao, *et al.*, Unidirectional Wetting Properties on Multi-Bioinspired Magnetocontrollable Slippery Microcilia, *Adv. Mater.*, 2017, **29**, 1–6.
127. Y. Lin, *et al.*, Magnetically Induced Low Adhesive Direction of Nano/Micropillar Arrays for Microdroplet Transport, *Adv. Funct. Mater.*, 2018, **28**, 1–6.
128. A. Al-Azawi, *et al.*, Slippery and magnetically responsive micropillared surfaces for manipulation of droplets and beads, *AIP Adv.*, 2020, **10**, 085021.
129. S. Ben, *et al.*, Multifunctional Magnetocontrollable Superwettable-Microcilia Surface for Directional Droplet Manipulation, *Adv. Sci.*, 2019, **6**, 1900834.